

# Densification of a-IGZO with low-temperature annealing for flexible electronics applications

J. G. Troughton, P. Downs, R. Price, and D. Atkinson

Citation: *Appl. Phys. Lett.* **110**, 011903 (2017); doi: 10.1063/1.4973629

View online: <http://dx.doi.org/10.1063/1.4973629>

View Table of Contents: <http://aip.scitation.org/toc/apl/110/1>

Published by the [American Institute of Physics](#)

---

## Articles you may be interested in

[Effects of substrate and anode metal annealing on InGaZnO Schottky diodes](#)

*Appl. Phys. Lett.* **110**, 011602011602 (2017); 10.1063/1.4973693

[Abnormal hump in capacitance–voltage measurements induced by ultraviolet light in a-IGZO thin-film transistors](#)

*Appl. Phys. Lett.* **110**, 023501023501 (2017); 10.1063/1.4973856

[Competing weak localization and weak antilocalization in amorphous indium–gallium–zinc-oxide thin-film transistors](#)

*Appl. Phys. Lett.* **110**, 022106022106 (2017); 10.1063/1.4974080

[Localized tail state distribution and hopping transport in ultrathin zinc-tin-oxide thin film transistor](#)

*Appl. Phys. Lett.* **110**, 023504023504 (2017); 10.1063/1.4973992

---



Small Conferences. BIG Ideas.

Applied Physics Reviews

SAVE THE DATE!

**3D Bioprinting: Physical and Chemical Processes**

May 2–3, 2017 • Winston Salem, NC, USA

## Densification of a-IGZO with low-temperature annealing for flexible electronics applications

J. G. Troughton,<sup>1,2</sup> P. Downs,<sup>2</sup> R. Price,<sup>2,a)</sup> and D. Atkinson<sup>1,b)</sup>

<sup>1</sup>Department of Physics, Durham University, Durham DH1 3LE, United Kingdom

<sup>2</sup>PragmatIC Printing Ltd., National Centre for Printable Electronics, NETPark, Sedgefield TS21 3FG, United Kingdom

(Received 21 September 2016; accepted 22 December 2016; published online 4 January 2017)

Amorphous InGaZnO (a-IGZO) thin-film transistors are a leading contender for active channel materials in next generation flat panel displays and flexible electronics. Improved electronic functionality has been linked to the increased density of a-IGZO, and while much work has looked at high-temperature processes, studies at temperatures compatible with flexible substrates are needed. Here, compositional and structural analyses show that short term, low-temperature annealing (<6 h) can increase the density of sputtered a-IGZO by up to 5.6% for temperatures below 300 °C, which is expected to improve the transistor performance, while annealing for longer times leads to a subsequent decrease in density due to oxygen absorption. *Published by AIP Publishing.*  
[\[http://dx.doi.org/10.1063/1.4973629\]](http://dx.doi.org/10.1063/1.4973629)

Amorphous oxide semiconductors (AOSs), spearheaded by amorphous Indium Gallium Zinc Oxide (a-IGZO), are regarded as one of the leading candidates for next generation thin-film transistor (TFT) active channel materials,<sup>1–5</sup> with emerging applications in flat-panel displays, flexible electronics, and low cost connectivity.<sup>6</sup> a-IGZO is considered a prime candidate for these applications due to its relatively high electron mobilities >10 cm<sup>2</sup>/Vs,<sup>2</sup> its good uniformity over large areas, its high optical transmission, above 75% over the visible range,<sup>7–9</sup> and its low processing temperatures, <200 °C.<sup>10</sup> To demonstrate the applicability of a-IGZO, several prototype devices have already been produced, including both rigid and flexible active matrix organic light emitting diode (AMOLED) displays,<sup>11–13</sup> e-ink displays,<sup>14–16</sup> and radio frequency identification (RFID) tags.<sup>17–19</sup>

The deposition of a-IGZO has been investigated through several routes, including pulsed laser deposition (PLD),<sup>2,20</sup> solution processing,<sup>21–23</sup> atomic layer deposition (ALD),<sup>24</sup> and sputtering.<sup>8,10,21,25–28</sup> It is commonly found that high-temperature post-process annealing has a positive impact on device performance. This has been attributed to several factors, including improvements in the bulk channel region, increasing field effect mobility ( $\mu$ ),<sup>25</sup> and decreasing sub-threshold slope (SS), and to improvements in the channel/gate dielectric interface.<sup>23,26,27,29</sup> The mechanisms for these improvements have been theoretically studied using density functional theory, looking at both the isolated channel and at the channel/gate dielectric interface. This has shown that when the channel region contains oxygen vacancies, these act as charge trapping sites causing both a reduction in  $\mu$  and an increase in SS, while structural relaxation from annealing allows these vacancies to either migrate towards indium atoms<sup>30</sup> or combine with under-coordinated oxygen atoms to create a stoichiometric local environment.<sup>31</sup> It has also been shown that truly stoichiometric channel/gate insulator

interfaces do not show any trapping sites, but that the introduction of defects at this interface induces charge trapping, the effect of which can be significantly reduced through annealing.<sup>32,33</sup> In both the channel and the interface studies, the presence of oxygen vacancies has been accompanied by metal-metal bonds and has been shown to be more common where the cells studied have been larger, i.e., the material has a lower density. Additionally, there are numerous works in which increases in density have been correlated to improvements in device performance, supporting this theoretical work, achieved through variations in deposition parameters.<sup>34–36</sup> It is therefore possible to monitor the reduction of these defects by measurement of the material density as a function of annealing. While the effect of higher temperature annealing, >250 °C, on the electronic properties and on material structure, has been well explored,<sup>27,28,37</sup> the impact of low- and intermediate-temperature annealing (<300 °C), compatible with fabrication of TFTs on flexible substrates, has received little attention, particularly in relation to the temporal aspect. Specifically, substrates such as polyethylene terephthalate (PET) or polyimide are relevant here, and the lower temperature annealing treatments are complementary to the low temperatures used to deposit the functional electronic materials on such substrates. It is this flexible application of a-IGZO TFTs that is likely to lead to the biggest market growth as the flexible electronics industry grows. Predictions for the general flexible electronics market run to values greater than \$300B by 2025,<sup>6</sup> with a significant proportion of this made up of devices in which a-IGZO could be a key material, suggesting that the development of understanding of the effects of low-temperature treatments on material properties is vital.

This work reports a detailed compositional and structural analysis of a-IGZO thin films as a function of thermal annealing time ( $t_{ann}$ ) and temperature ( $T_{ann}$ ), combining x-ray photoelectron spectroscopy (XPS), to study the chemical composition, and grazing incidence x-ray reflectivity (XRR), to probe the density, thickness, and interface structure of the thin-film material.

<sup>a)</sup>Electronic mail: richard@pragmaticprinting.com

<sup>b)</sup>Electronic mail: del.atkinson@durham.ac.uk

TABLE I. Density of a-IGZO with annealing at different temperatures ( $\text{g cm}^{-3}$ ).

| Temperature \ Time | 0 h             | 1 h             | 3 h             | 6 h             | 12 h            | 24 h            | 36 h            |
|--------------------|-----------------|-----------------|-----------------|-----------------|-----------------|-----------------|-----------------|
| 150 °C             | $5.96 \pm 0.06$ | $6.16 \pm 0.05$ | $6.14 \pm 0.08$ | $6.17 \pm 0.07$ | $6.14 \pm 0.09$ | $6.17 \pm 0.09$ | $6.10 \pm 0.06$ |
| 200 °C             | $5.96 \pm 0.06$ | $6.22 \pm 0.05$ | $6.29 \pm 0.09$ | $6.23 \pm 0.06$ | $6.23 \pm 0.06$ | $6.18 \pm 0.08$ | $6.12 \pm 0.09$ |
| 250 °C             | $5.96 \pm 0.06$ | $6.22 \pm 0.06$ | $6.20 \pm 0.07$ | $5.98 \pm 0.08$ | $5.96 \pm 0.07$ | $5.93 \pm 0.04$ | $5.89 \pm 0.11$ |
| 300 °C             | $5.96 \pm 0.06$ | $5.86 \pm 0.11$ | $5.88 \pm 0.06$ | $5.82 \pm 0.08$ | $5.87 \pm 0.07$ | $5.83 \pm 0.13$ | $5.80 \pm 0.14$ |

Here, 20 nm a-IGZO films were prepared by pulsed DC magnetron sputtering at room temperature, onto single crystal silicon substrates, with a native silicon dioxide layer, from a ceramic Indium Gallium Zinc Oxide target with atomic ratio of 1:1:1:4. Films were deposited with a DC sputter power of 1560 W and 1  $\mu\text{s}$  reverse bias pulses at a frequency of 250 Hz. The base pressure of the sputter system was 50  $\mu\text{Torr}$ , and the working gas was an argon and oxygen mixture (5% oxygen) that was introduced at 90 sccm with a working pressure of 2 mTorr. Single crystal silicon with native oxide was used here as the substrate to facilitate accurate and precise XRR measurements of density, and to eliminate the absorption of oxygen (or other contaminants) by the IGZO from the substrate.

The samples were annealed in ambient atmospheric conditions at four temperatures, 150 °C, 200 °C, 250 °C, and 300 °C, for times between 1 and 36 hours.

Compositional analysis of the as-deposited samples was done using XPS following argon ion cluster beam milling, intended to remove residual hydrocarbon contamination from the sample surface.

Structural analysis was done using XRR and the film thickness, density, surface structure width, and  $\text{SiO}_2/\text{a-IGZO}$  interface width were studied. XRR measurements were undertaken on a Bede D1 High Resolution X-Ray Diffractometer, using monochromated  $\text{Cu K}\alpha_1$  radiation (1.5406 Å). The XRR data were interpreted with best fitting simulations of a three layer model consisting of  $\text{Si}/\text{SiO}_2/\text{IGZO}$ , fitted using the GenX software package.<sup>38</sup> The IGZO stoichiometry used in the XRR analysis was obtained from XPS analysis. It should be noted that assuming ion charges of  $\text{In}^{3+}$ ,  $\text{Ga}^{3+}$ ,  $\text{Zn}^{2+}$ , and  $\text{O}^{2-}$ , and using the charge neutrality condition, the stoichiometric oxygen content in a film of  $\text{In}_w\text{Ga}_x\text{Zn}_y\text{O}_z$  is  $z = 1.5w + 1.5x + y$ .

Compositional analysis, using XPS, of the unannealed sample showed the atomic ratio in the deposited film to be 1:1.18:0.91:3.05 In:Ga:Zn:O. As discussed above, the stoichiometric oxygen content can be calculated from the ratio of the metal ions, and is found here to be  $z = 4.18$ , indicating that the deposited film, with  $z = 3.05$ , is oxygen deficient.

Figure 1(a) shows the full XRR profile for an unannealed sample along with the best fitting simulation from GenX, which shows that the measurements and the model fitted are in very close agreement. The critical angle  $\theta_c$  marked in this figure, is directly related to the density of this a-IGZO film, while the spacing of the Kiessig fringes gives a measure of the film thickness, and the rate of attenuation of the signal with angle relates to the structure of the film surface (the combined width of topological roughness and chemical grading between the sample and air) and the  $\text{SiO}_2/\text{IGZO}$  interface.<sup>39</sup> Figures 1(b) and 1(c) show linear intensity plots around the critical angle from the best fitting model that pertain to samples annealed at 200 °C. The positive shift to higher  $\theta_c$  indicates an increase in the IGZO density, compared to the  $t_{\text{ann}} = 0$  h, for annealing up to  $t_{\text{ann}} = 3$  h, while the negative shift to lower  $\theta_c$  for  $t_{\text{ann}} > 3$  h indicates a reduction in density. The best fitting simulations of the XRR data indicated no significant variation in either surface structure width  $4.4 \pm 0.8$  Å or  $\text{SiO}_2/\text{IGZO}$  interface width  $1.3 \pm 0.7$  Å (see [supplementary material](#), Tables S2 and S3) for all combinations of  $t_{\text{ann}}$  and  $T_{\text{ann}}$ , indicating that these interfaces are unaffected by annealing within the temperature range studied here.

Figure 2 and Table I both show the density of the IGZO as a function of annealing time obtained from the best fitting simulations to the XRR data. It is observed that annealing temperatures below 300 °C appear to cause an initial

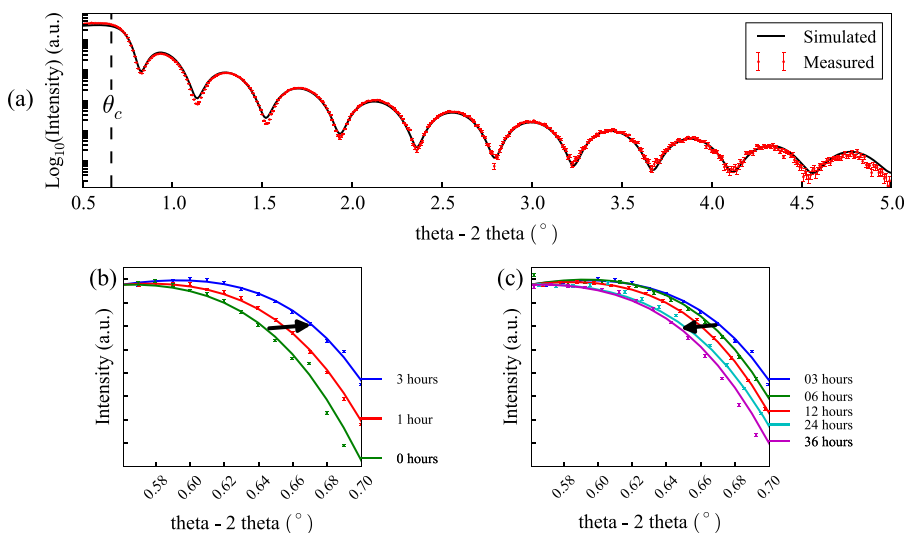


FIG. 1. (a) Measured and simulated XRR data for 20 nm a-IGZO film with the critical angle,  $\theta_c$ , marked for illustration. At angles greater than  $5^\circ$  the data becomes too noisy to fit. (b) and (c) The XRR fits for samples annealed at 200 °C from 0 to 36 h with  $\theta_c$  for each sample marked (here  $\theta_c$  is defined as then the intensity falls by 10% of the maximum). From 0 to 3 h, there is a positive shift in  $\theta_c$ , (b), while from 3 to 36 h there is a negative shift in  $\theta_c$ . (c).

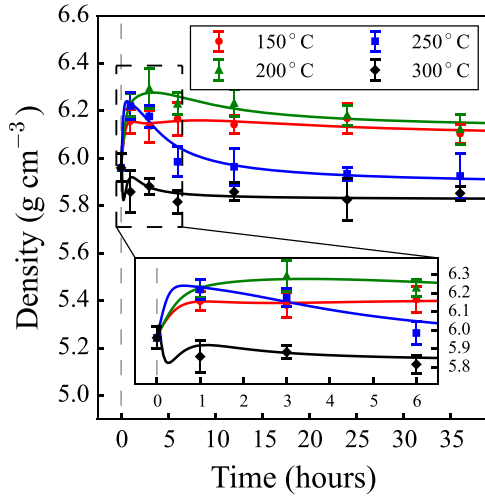


FIG. 2. Density of samples with annealing time shown for four different annealing temperatures, fitted with a model consisting of an exponentially decaying increase and an exponentially decaying decrease. Error bars represent one standard deviation in the value measured.

densification of the film, followed by a gradual decrease, while at 300 °C there is no increase. The annealing dependence of the density can be understood in terms of a thermal activation model with two parts. These two competing processes can be represented by an initial “stretched” exponential, as proposed by Moynihan *et al.* for the densification of amorphous solids,<sup>40,41</sup> followed by an exponential reduction of the density for longer annealing times attributed to absorption of oxygen. The solid lines in Figure 2 represent this model as described by the following equation:

$$\rho(t) = \rho_0 + \Delta\rho_s \left( 1 - \exp\left[\frac{-t}{\tau_s}\right]^\beta \right) - \Delta\rho_o \exp\left[\frac{-t}{\tau_o}\right], \quad (1)$$

where  $\rho(t)$  is the density after anneal time  $t$ ,  $\rho_0$  is the as-deposited density,  $\Delta\rho_s$  is the change in density due to structural relaxation,  $\tau_s$  is the characteristic time for this structural relaxation, the exponent  $\beta$  is inversely proportional to the width of the distribution of relaxation times ( $0 < \beta \leq 1$ ),  $\Delta\rho_o$  is the change in density due to oxygen absorption, and  $\tau_o$  is the characteristic time for this oxygen absorption.

The first process occurring during annealing and dominant at lower temperatures and short times is structural relaxation within the film accommodating defects produced during sample preparation; this causes densification of the film, as observed in other cases,<sup>37,42</sup> while at longer anneal times and higher temperatures, the process of oxygen absorption into the film increases (see Refs. 43 and 44). This process moves the oxygen ratio towards the “ideal” ratio of 1:1.18:0.91:4.18 as discussed earlier. From fitting of Equation (1) to the annealing time dependence of the density, information on the processes occurring during annealing can be extracted, in particular, the characteristic times for relaxation and oxygen absorption ( $\tau_s$  and  $\tau_o$ ), as well as the potential change in density due to each of these effects ( $\Delta\rho_s$ ,  $\Delta\rho_o$ ), these are presented in Table II. These parameters are of particular interest as they provide a guide for optimum

TABLE II. Characteristic times and changes in density from fitting equation (1) to data in Fig. 2.

|        | $\tau_s$ (h) | $\Delta\rho_s$ (g cm <sup>-3</sup> ) | $\tau_o$ (h) | $\Delta\rho_o$ (g cm <sup>-3</sup> ) |
|--------|--------------|--------------------------------------|--------------|--------------------------------------|
| 150 °C | 2.53         | 0.73                                 | 2.00         | 0.60                                 |
| 200 °C | 1.67         | 0.76                                 | 2.00         | 0.66                                 |
| 250 °C | 0.91         | 1.00                                 | 1.01         | 1.08                                 |
| 300 °C | 0.40         | 1.33                                 | 0.10         | 1.46                                 |

processing conditions. Table II shows that  $\tau_s$  falls linearly with temperature, while  $\Delta\rho_s$  shows a moderate increase over this range, indicating that structural relaxation occurs at all annealing temperatures, and that higher temperatures accelerate this process. This is unsurprising as there is likely a range of relaxation mechanisms with a range of barrier energies. Conversely,  $\tau_o$  is constant between 150 °C and 200 °C and then falls rapidly, while  $\Delta\rho_o$  is also constant up to 200 °C, before increasing at higher temperatures. This suggests that the process of oxygen absorption is thermally activated and becomes more significant at temperatures above 200 °C.

While the change in densities seen here is significant and well above the measurement error margin, it should be noted that the change in sample thickness is small, and in most cases, the measured thickness is within the error margin of that of the un-annealed sample. This apparent lack of change in thickness may be explained by the competing processes discussed above. While the structural relaxation process would be expected to cause a reduction in film thickness, the absorption of oxygen may work, in complement to the decrease in density, to increase the thickness. Given the small density range over which these two processes work, it is reasonable to conclude that they work together to reduce the change in thickness to below the measurement noise. Indeed the only films in which a decrease in thickness was seen are those annealed at 200 °C, where the energy barrier to oxygen absorption is significant, but structural relaxation occurs, in which case the maximum density was found after 3 h of annealing and the corresponding thickness of the layer dropped from  $20.13 \pm 0.15$  nm to  $19.68 \pm 0.13$  nm. At other temperatures, the thickness varied within  $\pm 0.15$  nm of the initial thickness.

A potential alternative reason for the fall in density at 300 °C could be decomposition and subsequent desorption of material in the film, particularly of the Zn-O, due to the low electron affinity of zinc. However, it has been shown, through thermal desorption spectroscopy, that significant desorption of zinc only occurs above 300 °C, and therefore, this process is unlikely to have a significant impact here.<sup>45</sup> Finally, it should be noted that the crystallization behavior of a-IGZO has been well studied elsewhere, and the onset of crystallization does not occur until between 520 °C and 650 °C,<sup>28,37</sup> therefore, crystallographic changes are highly unlikely to have affected the materials studied here.

From this work, the annealing condition that led to the greatest increase in density, 1 h annealing at 200 °C, was implemented in coplanar top-gated transistor device structures, with multiple channel length:width ratios, on a

polyimide substrate, with the annealing taking place after deposition of the IGZO and before any further processing. After performing I–V transfer sweeps between  $-6$  V and  $+6$  V, it was found that the annealed devices, when compared to similarly fabricated devices without the annealing step, showed significant improvement in the parameters discussed, consistent with the reduction of defects in the IGZO channel and interface. These improvements are summarised in Table S5 of the [supplementary material](#), and include average reduction in sub-threshold slope (SS) of around 23%, increase in mobility of around 22%, shift of  $V_{on}$  towards 0 V by 10%, and reduction in hysteresis by 45%, although this does include some asymmetry between forward and reverse sweeps, as detailed in Table S5 ([supplementary material](#)).

In summary, a detailed structural and compositional study of amorphous InGaZnO as a function of time at relatively low annealing temperatures has shown that two phenomena affect a-IGZO thin films during annealing; these are structural relaxation and oxygen absorption. It is shown that structural relaxation proceeds at temperatures between  $150^\circ\text{C}$  and  $300^\circ\text{C}$ , with the rate and magnitude dependent on the annealing temperature, while oxygen absorption is minimal below  $200^\circ\text{C}$  but increase in both rate and magnitude above this temperature. These processes are understood in terms of energy barriers with a range of energies for both the relaxation process and the oxygen absorption, where the minimum energy barrier for relaxation is below  $36$  meV (the thermal energy,  $k_B T$ , at  $150^\circ\text{C}$ ) with a continuous distribution above this energy, while the energy barrier minimum for oxygen absorption is around  $40$  meV (thermal energy at  $200^\circ\text{C}$ ) with a continuous distribution above this. These energy barriers are seen here for material that is initially oxygen depleted, requiring around one oxygen per unit cell to achieve stoichiometry, and so the energy requirements are likely to change for other stoichiometries. Here a maximum densification of 5.6% from the as-deposited material was achieved at  $200^\circ\text{C}$  (where structural relaxation is able to proceed, while minimal oxygen is absorbed). Finally it should be noted that, as this study is concerned primarily with the changes in the bulk IGZO material, and the absorption of oxygen through the top surface, the conclusions drawn here, although taken from samples produced on a silicon substrate, are applicable to any other flexible or non-flexible substrate. Considered within the realm of a-IGZO TFT fabrication, these results provide strong guidance for mid-process annealing, whereby the density of a-IGZO can be increased, and the oxygen stoichiometry improved, without affecting other material layers.

See [supplementary material](#) for the extended version of Table II and complete XRR parameter tables.

This work was supported by a Knowledge Transfer Partnership, funded by Innovate UK. XPS data were provided by Kratos, Ltd., and material samples were fabricated by Pragmatic Printing, Ltd. The authors would also like to thank Brian Tanner for his invaluable assistance with the x-ray measurement analysis.

- <sup>1</sup>K. Nomura, H. Ohta, K. Ueda, T. Kamiya, M. Hirano, and H. Hosono, *Science* **300**(5623), 1269 (2003).
- <sup>2</sup>K. Nomura, H. Ohta, A. Takagi, T. Kamiya, M. Hirano, and H. Hosono, *Nature* **432**(7016), 488 (2004).
- <sup>3</sup>T. Kamiya and H. Hosono, *Int. J. Appl. Ceram. Technol.* **2**(4), 285 (2005).
- <sup>4</sup>J. S. Park, W. J. Maeng, H. S. Kim, and J. S. Park, *Thin Solid Films* **520**(6), 1679 (2012).
- <sup>5</sup>E. Fortunato, P. Barquinha, and R. Martins, *Adv. Mater.* **24**(22), 2945 (2012).
- <sup>6</sup>D. Gamota, M. Joyce, A. Schaller, and J. Zhang, "Large area flexible electronics," in *iNEMI Roadmap 2015* (2015).
- <sup>7</sup>A. Suresh, P. Gollakota, P. Wellenius, A. Dhawan, and J. F. Muth, *Thin Solid Films* **516**(7), 1326 (2008).
- <sup>8</sup>Y. Kikuchi, K. Nomura, H. Yanagi, T. Kamiya, M. Hirano, and H. Hosono, *Thin Solid Films* **518**(11), 3017 (2010).
- <sup>9</sup>J. Liu, D. B. Buchholz, J. W. Hennek, R. P. H. Chang, A. Facchetti, and T. J. Marks, *J. Am. Chem. Soc.* **132**(34), 11934 (2010).
- <sup>10</sup>H. Yabuta, M. Sano, K. Abe, T. Aiba, T. Den, H. Kumomi, K. Nomura, T. Kamiya, and H. Hosono, *Appl. Phys. Lett.* **89**(11), 112123 (2006).
- <sup>11</sup>C. J. Kim, D. Kang, I. Song, J. C. Park, H. Lim, S. Kim, E. Lee, R. Chung, J. C. Lee, and Y. Park, in *International Electron Devices Meeting* (2006), p. 1.
- <sup>12</sup>J. K. Jeong, J. H. Jeong, J. H. Choi, J. S. Im, S. H. Kim, H. W. Yang, K. N. Kang, K. S. Kim, T. K. Ahn, H.-J. Chung, M. Kim, B. S. Gu, J.-S. Park, Y.-G. Mo, H. D. Kim, and H. K. Chung, *SID Int. Symp. Dig. Tech.* **39**(1), 1 (2008).
- <sup>13</sup>Y. G. Mo, M. Kim, and H. D. Kim, *J. Soc. Inf. Disp.* **19**(1), 16 (2011).
- <sup>14</sup>M. Ito, M. Kon, M. Ishizaki, and N. Sekine, in *Proceedings of the IDW/AD'05* (2005), p. 845.
- <sup>15</sup>M. Ito, M. Kon, C. Miyazaki, N. Ikeda, M. Ishizaki, Y. Ugajin, and N. Sekine, *IEICE Trans. Electron.* **E90-C**(11), 2105 (2007).
- <sup>16</sup>M. Ito, M. Kon, C. Miyazaki, N. Ikeda, M. Ishizaki, R. Matsubara, Y. Ugajin, and N. Sekine, *Phys Status Solidi A* **205**(8), 1885 (2008).
- <sup>17</sup>H. Ozaki, T. Kawamura, H. Wakana, T. Yamazoe, and H. Uchiyama, *IEICE Electron. Express* **8**(4), 225 (2011).
- <sup>18</sup>B. D. Yang, J. M. Oh, H. J. Kang, S. H. Park, C. S. Hwang, M. K. Ryu, and J. E. Pi, *ETRI J.* **35**(4), 610 (2013).
- <sup>19</sup>K. Myny, A. K. Tripathi, J.-L. van der Steen, and B. Cobb, *IEEE Commun. Mag.* **53**(10), 182 (2015).
- <sup>20</sup>A. Suresh, P. Wellenius, A. Dhawan, and J. Muth, *Appl. Phys. Lett.* **90**(12), 123512 (2007).
- <sup>21</sup>J. H. Lim, J. H. Shim, J. H. Choi, J. Joo, K. Park, H. Jeon, M. R. Moon, D. Jung, H. Kim, and H. J. Lee, *Appl. Phys. Lett.* **95**(1), 012108 (2009).
- <sup>22</sup>K. K. Banger, Y. Yamashita, K. Mori, R. L. Peterson, T. Leedham, J. Rickard, and H. Sirringhaus, *Nat. Mater.* **10**(1), 45 (2011).
- <sup>23</sup>Y. S. Rim and H. J. Kim, *Phys Status Solidi A* **211**(9), 2195 (2014).
- <sup>24</sup>A. Illiberi, B. Cobb, A. Sharma, T. Grehl, H. Brongersma, F. Roozeboom, G. Gelinck, and P. Poodt, *ACS Appl. Mater. Interfaces* **7**(6), 3671 (2015).
- <sup>25</sup>S. J. Jeon, J. W. Chang, K. S. Choi, J. P. Kar, T. I. Lee, and J. M. Myoung, *Mater. Sci. Semicond. Process.* **13**(5–6), 320 (2010).
- <sup>26</sup>H. Q. Chiang, B. R. McFarlane, D. Hong, R. E. Presley, and J. F. Wager, *J. Non-Cryst. Solids* **354**(19–25), 2826 (2008).
- <sup>27</sup>T. Kamiya, K. Nomura, and H. Hosono, *Sci. Technol. Adv. Mater.* **11**(4), 1 (2010).
- <sup>28</sup>K. Ide, K. Nomura, H. Hiramatsu, T. Kamiya, and H. J. Hosono, *Appl. Phys.* **111**(7), 073513 (2012).
- <sup>29</sup>M. D. H. Chowdhury, S. H. Ryu, P. Migliorato, and J. Jang, *J. Appl. Phys.* **110**(11), 114503 (2011).
- <sup>30</sup>H.-K. Noh, K. J. Chang, B. Ryu, and W.-J. Lee, *Phys. Rev. B* **84**(11), 115205 (2011).
- <sup>31</sup>W. Körner, D. F. Urban, and C. Elsässer, *Phys. Status Solidi A* **212**(7), 1476 (2015).
- <sup>32</sup>H. Song, Y. Kang, H.-H. Nahm, and S. Han, *Phys. Status Solidi B* **252**(8), 1872 (2015).
- <sup>33</sup>M. D. H. Chowdhury, J. G. Um, and J. Jang, *Appl. Phys. Lett.* **105**(23), 233504 (2014).
- <sup>34</sup>M. P. Hung, D. Wang, T. Toda, J. Jiang, and M. Furuta, *ECS J. Solid State Sci. Technol.* **3**(9), Q3023 (2014).
- <sup>35</sup>J. Grochowski, Y. Hanyu, K. Abe, J. Kaczmarek, J. Dyczewski, H. Hiramatsu, H. Kumomi, H. Hosono, and T. Kamiya, *J. Disp. Technol.* **11**(6), 523 (2015).
- <sup>36</sup>K. Jeon, C. Kim, I. Song, J. Park, S. Kim, S. Kim, Y. Park, J. H. Park, S. Lee, D. M. Kim, and D. H. Kim, *Appl. Phys. Lett.* **93**(18), 182102 (2008).
- <sup>37</sup>K. Nomura, T. Kamiya, H. Ohta, K. Shimizu, M. Hirano, and H. Hosono, *Phys. Status Solidi A* **205**(8), 1910 (2008).
- <sup>38</sup>M. Björck and G. Andersson, *J. Appl. Crystallogr.* **40**(6), 1174 (2007).

- <sup>39</sup>M. Wormington, *Philos. Mag. Lett.* **74**(3), 211 (1996).
- <sup>40</sup>C. T. Moynihan, P. B. Macedo, C. J. Montrose, C. J. Montrose, P. K. Gupta, M. A. DeBolt, J. F. Dill, B. E. Dom, P. W. Drake, A. J. Easteal, P. B. Elterman, R. P. Moeller, H. Sasabe, and J. A. Wilder, *Ann N. Y. Acad. Sci.* **279**(1 The Glass Tra), 15 (1976).
- <sup>41</sup>J. Málek and J. Šhánělová, *J. Therm. Anal. Calorim* **60**(3), 975 (2000).
- <sup>42</sup>K. Nomura, A. Takagi, T. Kamiya, H. Ohta, M. Hirano, and H. Hosono, *Jpn. J. Appl. Phys.* **45**(5B), 4303 (2006).
- <sup>43</sup>K. H. Ji, Kim, J.-I., H. Y. Jung, S. Y. Park, R. Choi, U. K. Kim, C. S. Hwang, D. Lee, H. Hwang, and J. K. Jeong, *Appl. Phys. Lett.* **98**(10), 103509 (2011).
- <sup>44</sup>C.-S. Fuh, P.-T. Liu, Y.-T. Chou, L.-F. Teng, and S. M. Sze, *ECS J. Solid State Sci.* **2**(1), Q1 (2013).
- <sup>45</sup>A. Hino, Y. Takanashi, H. Tao, S. Morita, M. Ochi, H. Goto, K. Hayashi, and T. Kugimiya, *J. Vac. Sci. Technol., B* **32**(3), 031210 (2014).